Reflectance Modeling of Snow-Covered Forests in Hilly Terrain

Dagrun Vikhamar, Rune Solberg, and Klaus Seidel

Abstract

Seasonal snow covers large land areas of the Earth. Information about the snow extent in these regions is important for climate studies and water resource management. A linear spectral mixture model for snow-covered forests (the SnowFor *model) has previously been developed for flat terrain. The* SnowFor *model includes reflectance components for snow, trees and snow-free ground. In this paper, the model is extended to handle radiometric effects caused by topography on mixed pixels of snow and trees through subpixel topographic reflectance modeling. Empirical reflectance models for snow and trees, based on the local solar incidence angle, are proposed (*TopoSnow *and* TopoTree *models), and integrated into the* SnowFor *model. Experiments with two Landsat Thematic Mapper (TM) images are carried out in hilly, forested terrain in Alptal, Switzerland with full snow cover. Results show that the calibrated* TopoSnow *and* TopoTree *models enhance the modeling of reflectance variability from snow-covered forests for visible and near-infrared wavelengths. The performance of four other topographic correction methods is evaluated for snow-covered forests.*

Introduction

Seasonal snow covers large areas of the Earth's land surface. Information about snow is important for climate studies (Cess, *et al.*, 1991) and hydrological applications. Snowmelt may contribute significantly to the runoff from drainage basins, and runoff forecasts serve flood warning and hydropower production (Winther and Hall, 1999). Therefore, improving the techniques for monitoring the snow cover is of growing interest.

Remote sensing techniques have far reaching monitoring potential. Methods for snow-cover mapping have been developed for optical sensors (e.g., Andersen, 1982; Hall, *et al.*, 1995; Rosenthal and Dozier, 1996) for active microwave sensors (e.g., Koskinen, *et al.*, 1997; Nagler and Rott, 2000) and for passive microwave sensors (e.g., Hallikainen, 1989; Foster, *et al.*, 1997). Presently, the reflected signals from snow-covered areas recorded by optical sensors are better understood than those acquired by microwave sensors (Solberg, *et al.*, 1997). Hence, optical images are most frequently used in operational snow-cover mapping, although clouds may obscure the mapping (Solberg and Andersen, 1994; Hall, *et al.*, 2002). Snow in forests is challenging to map with optical remote sensing techniques because some of the snow is masked by the tree canopy and thereby mostly occluded from the sensor. Additionally, the trees contribute spectrally to the satellite-measured radiance. A few studies have particularly focused on handling the forest problem (Klein, *et al.*, 1998; Metsämäki, *et al.*, 2002), and it has been demonstrated that snow in forests is mapped with lower accuracy than in unforested regions (Hall, *et al.*, 2001).

To investigate the problems of snow-cover mapping in forests, a linear spectral mixture model (*SnowFor*) has previously been developed for different forest types with snow-covered ground and flat terrain (Vikhamar and Solberg, 2002 and 2003b). It is known that topography significantly influences the radiometry of the acquired satellite image (Proy, *et al.*, 1989). There are two objectives for the work presented in this paper: 1) To study radiometric effects caused by the topography in snow-covered forested areas; and 2) To model these topographic effects in *SnowFor*. The *SnowFor* model is the main component of a snow-cover mapping method for forests currently under development. Reflectance modeling is a step on the way to understand processes, and thereby being able to improve subpixel snow cover mapping. For this study, two Landsat TM images of hilly, forested terrain in Switzerland are selected for experiments. The 30 m spatial resolution makes it possible to identify and study pure snow and forest pixels. Empirical reflectance models for snow and trees, based on the local solar incidence angle, are proposed (*TopoSnow* and *TopoTree*), and integrated into the *SnowFor* model. This approach, referred to as subpixel topographic reflectance modeling, was motivated by an experiment presented here which investigates the performance of four other topographic correction methods for snow-covered forests. Modeled and observed Landsat TM reflectances are compared for visible and near-infrared wavelengths.

The paper first provides a short summary of how trees and topography affect the image radiometry, and how terrain effects are handled by four topographic correction methods. Then, the approach for integrating radiometric terrain effects into the *SnowFor* model is presented (Figure 1). Moreover, the study area, data sets, and four experiments are successively described. Finally, the result of the reflectance modeling is assessed.

Background

Effects influencing the measured radiance from snow-covered forests, and how terrain effects are handled by four topographic correction methods, are briefly described in the following.

D. Vikhamar is with the Department of Geosciences, University of Oslo, P.O. Box 1047 Blindern, N-0316 Oslo, Norway (dagrunv@geo.uio.no).

R. Solberg is with the Norwegian Computing Center, P.O. Box 114 Blindern, N-0314 Oslo, Norway (rune.solberg@nr.no).

Klaus Seidel is with the Remote Sensing Group, Computer Vision Lab (ETHZ), CH 8092 Zürich, Switzerland (seidel@vision.ee.ethz.ch).

Photogrammetric Engineering & Remote Sensing
Vol. 70, No. 9, September 2004, pp. 1069–1079.

0099-1112/04/7009–1069/$3.00/0

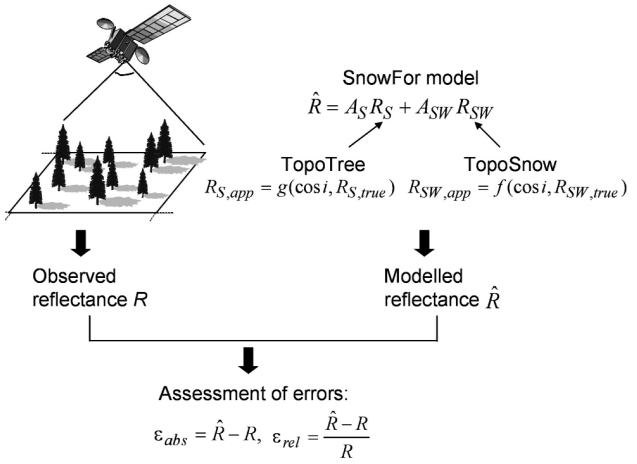

Figure 1. Flowchart depicting the reflectance modeling by the *SnowFor* model and the integration of the two topographic reflectance submodels, applied for spruce forests with full snow-cover.

Effects of Trees and Topography on Satellite-measured Radiance

The radiance measured by an optical satellite sensor is composed of radiance from the observed ground area (reflected direct and diffuse irradiance), and path radiance (an atmospheric component) (Richards, 1993). Trees and topography are two important factors affecting the direct and diffuse irradiance reaching the snow-covered ground. Therefore, trees and topography are described in this section.

Trees

Trees make a flat area three-dimensional, causing several shadow effects. In Vikhamar and Solberg (2003b), the shadow effects resulting from trees in flat terrain were divided into primary and secondary effects. Primary shadow effects are caused by single trees, and include the self-shadow in a tree crown and the cast shadow on the ground. Secondary shadow effects result from the surrounding trees, and include cast shadows on other trees and surfaces, as well as reduced ground-received diffuse irradiance caused by tree crowns shielding the sky hemisphere. The penetration of light through the canopy is determined by the tree-crown density, and thus the tree species, which in turn affect the shape of the cast shadow. Because the tree-crown density of leafless birch is significantly lower, much more light penetrates leafless birch than for pine and spruce. In sparse forests, shadows may cover a large fraction of the ground at low solar elevation angles. Yet, by increasing the crown coverage in simulations by Li and Strahler (1985), it was demonstrated that *viewable* shadowed areas on the forest floor actually decreased because larger areas became shaded tree crowns.

Topography

For mountainous terrain, Proy, *et al.* (1989) describe three effects caused by the topography: 1) Some areas receive exclusively diffuse irradiance due to cast shadows; 2) Shielding of the sky hemisphere reduces the diffuse irradiance; and 3) Surrounding terrain reflects irradiance towards the observed ground area. Similar effects arise when the mountainous terrain is forest covered. The shadowed areas in tree crowns and on the ground change location and spatial extent as compared to forested flat terrain. The shadowed areas become smaller on slopes facing the sun, while they increase on slopes oriented away from the sun (Gemmel, 1998).

TABLE 1. METHODS FOR TOPOGRAPHIC CORRECTION OF SATELLITE MEASURED RADIANCE (MEYER, ET AL., 1993). L_H AND L_T ARE RADIANCE OF FLAT AND SLOPING TERRAIN, RESPECTIVELY. $\overline{L}_T$ IS THE AVERAGE RADIANCE OF THE IMAGE PIXELS. $C = b/m$, WHERE m IS SLOPE AND b IS INTERCEPT OF THE REGRESSION EQUATION DERIVED FROM $\cos(i)$ AND L_T OF THE IMAGE PIXELS. sz IS THE SOLAR ZENITH ANGLE AND k IS THE MINNAERT CONSTANT

Method	Equation
Lambertian cosine correction	$L_H = L_T\left(\frac{\cos(sz)}{\cos(i)}\right)$
C-correction	$L_H = L_T\left(\frac{\cos(sz) + C}{\cos(i) + C}\right)$
Minnaert correction	$L_H = L_T\left(\frac{\cos(sz)}{\cos(i)}\right)^k$
Statistic-empirical correction	$L_H = L_T - \cos(i)m - b + \overline{L}_T$

Topographic Correction Methods

Several methods have been developed with the purpose of removing terrain effects from the measured pixel radiance. Widely used methods are the Lambertian cosine correction, the statistic-empirical correction, the C-correction, and the Minnaert correction (see Teillet, *et al.*, 1982; Meyer, *et al.*, 1993; Ekstrand, 1996). The general approach of these methods is to normalize the observed radiance from inclined surfaces to flat (horizontal) surfaces by modeling the local incidence angle to the terrain surface $\cos(i)$ for each pixel (Table 1). i is defined as the angle between the surface normal and the solar beam. Using information about the solar position at the acquisition time for the satellite image and the local terrain relief, i can be calculated for a pixel by the formula (Smith, *et al.*, 1980):

$$\cos i = \cos sz \cos tz + \sin sz \sin tz \cos(sa - ta), \qquad (1)$$

where sz is the solar zenith angle, sa is the solar azimuth angle, tz is the surface normal zenith angle or the terrain slope, and ta is the terrain azimuth angle.

The Lambertian cosine correction transforms the direct irradiance on an inclined terrain surface to a horizontal surface by assuming Lambertian reflection and ignoring the diffuse irradiance. A Lambertian surface reflects irradiance equally in all directions (diffuse reflector), which makes it independent of viewing angle, but still dependent on the solar incidence angle. The statistic-empirical correction and the C-correction assume a statistical linear relationship between the $\cos(i)$ and the radiance. Both methods attempt to capture direct and diffuse irradiance, and the linear relationship indicates that the methods should perform best for surfaces behaving as Lambertian reflectors. The Minnaert correction is an extension of the Lambertian model employing the Minnaert constant, k, which varies between 0 and 1 (Minnaert, 1941). The constant k is empirically determined for the actual surface, and its purpose is to handle non-Lambertian reflectors (anisotropic reflectors). When $k = 1$ it is a normal Lambertian cosine correction. Ekstrand (1996) proposed a variant of this correction method by letting k vary with the local solar incidence angle.

Other approaches for topographic corrections have been proposed by Pouch and Campagna (1990), Proy, *et al.* (1989), Gu and Gillespie (1998), and Dymond, *et al.* (2001).

Handling Terrain Effects in the *SnowFor* Model

This section first presents the *SnowFor* model and, secondly, describes a subpixel approach to handle terrain effects on mixed pixels of snow and trees. Terrain effects are not removed from the measured pixel reflectance, but rather included in the *SnowFor* model, by integrating topographic reflectance submodels for the spectral land-cover types within a pixel.

The *SnowFor* Model

A subpixel reflectance model for snow-covered forests (*SnowFor*) has previously been developed (Vikhamar and Solberg, 2002 and 2003b). Pixel reflectance is modeled as a linear mixture of snow, individual tree species and snow-free bare ground (e.g., rock, soil, low vegetation):

$$\hat{R} = A_P R_P + A_S R_S + A_B R_B + A_{SW} R_{SW} + A_{BG} R_{BG}, \qquad (2)$$

where $\hat{R}$ is the modeled pixel reflectance for a given wavelength λ and $A_P + A_S + A_B + A_{SW} + A_{BG} = 1$. A represents area fractions of a pixel and R is reflectance. The subscripts P, S and B refer to pine, spruce and birch tree crowns, respectively, while the subscripts SW and BG refer to snow and bare ground, respectively. So far, the work has focused on developing and validating the *SnowFor* model. Reflectance modeling makes it possible to study the various effects contributing to the observed pixel reflectance. Reflectance variability of some forest types with full snow coverage has been studied based on detailed single-tree modeling, and the importance of different shadow effects in flat terrain have been quantified.

The *SnowFrac* snow-cover mapping method is based on the *SnowFor* model proposed by Vikhamar and Solberg (2002 and 2003b). An algorithm suited for operational snow-cover mapping is currently under development (Vikhamar and Solberg, 2003a). The main concept of the *SnowFrac* method is described here to explain the use of the reflectance modeling. The snow-covered fraction of a pixel is estimated by spectral unmixing of multispectral data using the *SnowFor* model. An over-determined equation system is solved by the least-squares method to find the best fit of modeled reflectance values for a number of wavelengths (e.g., Schott, 1997, pp. 285–287). Since snow-cover fraction is the variable of interest, prior information about other land-cover types within each pixel is used for the spectral unmixing. Input parameters to the unmixing algorithm consist of both land-cover spectra and a land-cover fraction map, the latter containing area fractions of the forest types within a pixel. The purpose of specifying several input parameters is to improve the accuracy of the output snow-cover fraction by reducing the number of unknowns in the equation system. Therefore, a general requirement for the *SnowFrac* method is a pixel based land-cover fraction map.

Integrating Terrain Effects into the SnowFor Model

Because the basic concept of the *SnowFor* model is fractional reflectance modeling of spectrally separable land cover types (snow, trees, and bare ground) and radiometric terrain effects are assumed to be land cover dependent, terrain effects are proposed to be handled by reflectance models for individual land-cover types. These topographical submodels modify the apparent reflectance (at-satellite reflectance, not corrected for atmospheric and terrain effects) of individual land cover types according to the terrain relief derived from a digital terrain model.

As described in the background section, the main effects influencing the measured pixel radiance are reflected direct, and diffuse irradiance from the observed ground area and the path radiance. If path radiance is removed from the pixel radiance by an atmospheric correction method (e.g., Song, *et al.*, 2001), the primary reflected irradiance from a surface (land cover type) is the direct irradiance, which may be simplified to a parameterization of these two components: 1) The local solar incidence angle, i; and 2) The optical properties of the surface, L, described by its true reflectance, $R_{L,true}$. The viewing angle of the sensor is of importance if the surface is not a Lambertian reflector. The true reflectance modulated by radiometric terrain effects is here denoted terrain reflectance for a land-cover type, $R_{L,terr}$. A general topographic reflectance model for individual land-cover types based on a Lambertian model is used as starting point: $R_{L,terr} = \cos(i) R_{L,true}$ (Figure 2).

To extend the basic Lambertian model to better represent nature, the topographic reflectance model may be determined empirically by regression (linear or non-linear) of the $\cos(i)$ and the apparent reflectance values for given wavelengths and land cover type. For the experiments in this work with spruce forests and full snow cover, two land-cover topographic submodels for apparent reflectance are proposed, one for snow and one for spruce tree crowns: *TopoSnow*: $R_{SW,app} = f(\cos(i), R_{SW,true})$ and *TopoTree*: $R_{S,app} = g(\cos(i), R_{S,true})$, where f and g are empirically calibrated (determined) functions. Each submodel accounts for direct radiation (modeled by the local solar incidence angle) and true reflectance of a given land cover type which are considered the primary effects. The purpose of empirical calibration of these functions is to account for secondary effects, including reflected diffuse radiation, anisotropic reflectors, and natural reflectance variability within each land cover. If the empirical functions f and g are linear, both snow and spruce tree crowns are modeled as Lambertian reflectors, while a non-linear function may capture anisotropic reflectance characteristics. Cast shadows from surrounding terrain are not handled with the $\cos(i)$ model which solely accounts for the local terrain relief. Calibration of these empirical models is a key issue and is discussed in the experiments and results section.

The *TopoSnow* and the *TopoTree* models are merged into the *SnowFor* model as the reflectance component of snow and spruce tree crowns within a pixel (Figure 1). In this way the snow reflectance (R_{SW}) and the tree-crown reflectance (R_S) vary for each pixel in an image based on its local solar incidence angle.

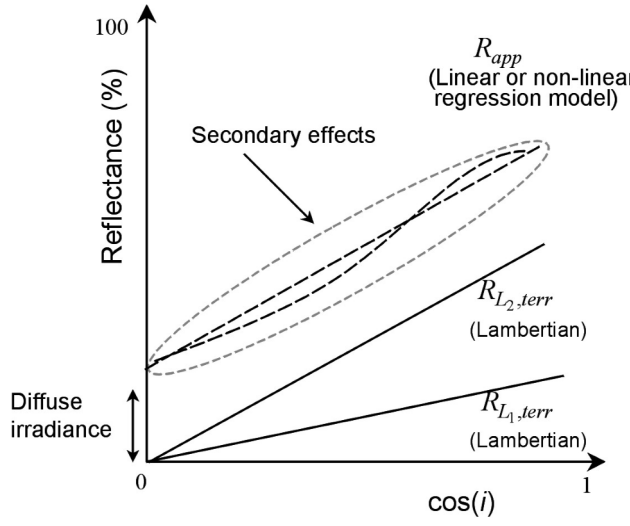

Figure 2. Concept of an empirical topographic reflectance model for individual land-cover types. A Lambertian model is used as starting point to account for direct irradiance and land-cover true reflectance (primary effects): $R_{L,terr} = \cos(i) R_{L,true}$. The figure illustrates two Lambertian models for land-cover types with different true reflectance ($R_{L2,true} > R_{L1,true}$). To include diffuse irradiance, anisotropic reflectance and natural reflectance variability within a land-cover type (secondary effects), the model is calibrated empirically by regression (linear or non-linear) of the cosine of the local solar incidence angle and the apparent reflectance values of a wavelength, for the particular land-cover type (dashed lines). A shift on the y-axis models the diffuse irradiance and other possible effects giving a background irradiance. A non-linear model accounts for some anisotropic reflectance.

Study Area and Data Set

The study area Alptal is located in the lower Alps, Canton Schwyz, Switzerland (47.1°N, 8.8°E) (Figure 3). Alptal is a valley surrounded by forested hills where the main tree species is Norway spruce (*Picea abies*). A small test site (2.76 km × 1.44 km) was identified based on conditions with full snow coverage and availability of an aerial photo for deriving a forest fraction map. The large variability in conifer forest density and in terrain relief (Figure 4) made the test site suitable to study terrain effects. The test site represents a transect from the valley bottom and across the ridge of a hill from 1073 to 1651 m. ASL.

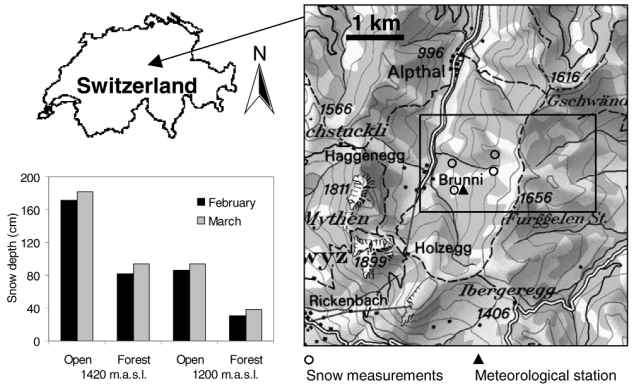

Figure 3. The study area in Alptal, Switzerland. Shaded areas on the map (original scale 1:200 000) are forests, and white areas are open fields. Reflectance modeling was carried out for the area within the black frame. A selection of open and forested sites outside the black frame served for calibration of the *TopoSnow* and the *TopoTree* models. The graph shows snow depths measured at four sites on 7, 10 and 15 February 2000 and 9, 13 and 15 March 2000.

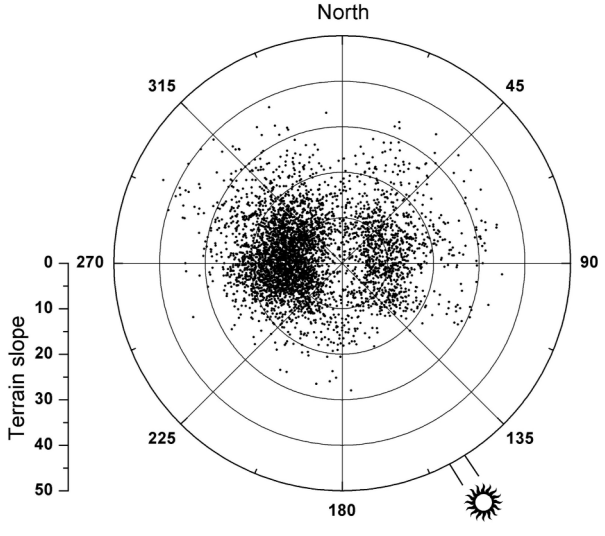

Figure 4. Polar plot of terrain exposition and slope (°) for the test site for 4416 Landsat TM pixels inside the black frame in Figure 3. The plot shows that most terrain expositions are represented, as well as terrain slopes up to 43°. Solar azimuth angles for the two Landsat TM scenes are depicted.

The data set consists of Landsat images, an aerial photo, a digital elevation model (DEM), snow measurements and meteorological observations. The use of high-resolution images facilitates identification of pixels of pure land cover types: snow and trees. To study different situations with full snow coverage and changing solar exposition, all cloud-free Landsat TM and ETM+ images (path 195, row 27) from the winter 2000 covering Alptal were selected. Due to sensor saturation for most of the snow surfaces in the visible and near-infrared channels (channels 1–4) of the ETM+ images, only two TM images (10 February and 13 March 2000) could be used. Sensor saturation of snow surfaces was to some extent found in the blue channel of the TM images (Channel 1), so this channel was also rejected.

The two TM images were geometrically converted to orthoimages, using digital maps (1:25000) and a DEM (25 m spatial resolution and 10 m height resolution). Radiometric calibration to apparent reflectance was carried out by empirical linear calibration models developed from satellite-measured radiance and spectra of dark and light objects (lake water and snow) in the scene (Schott, 1997, pp. 211–212). In situ spectra from the time of image acquisition were not available. However, spectra of snow, measured with a portable FieldSpec® FR spectroradiometer (ASD, 1996) on occasions with similar meteorological history as the TM scenes, were used. Lake reflectance was represented by tap water from the Johns Hopkins University Spectral Library (Salisbury, 2002). The calibration method implied a loss of the TM channels 5 and 7, due to the combined low water and low snow reflectance in mid-infrared wavelengths (Figure 5). The atmospheric conditions were assumed

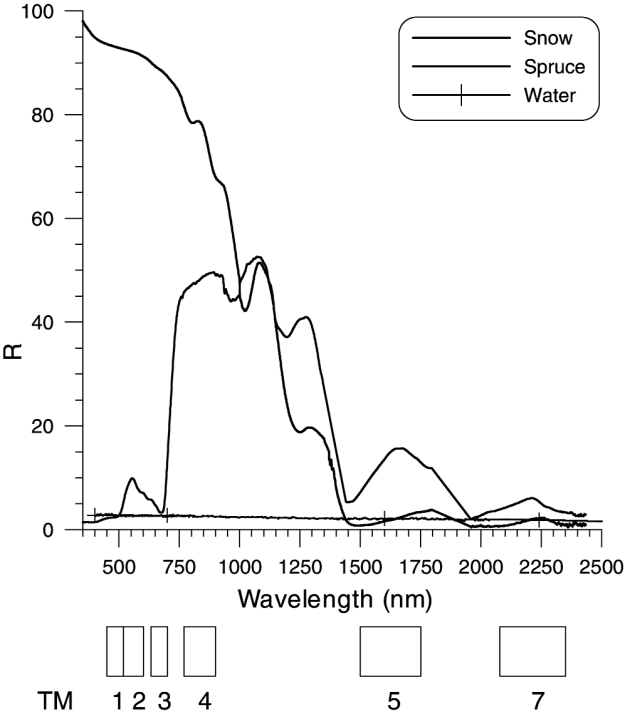

Figure 5. Spectra of snow, spruce tree-crowns and water. The Landsat TM channels 1–5 and 7 are depicted. Snow and water spectra were used for empirical linear calibration of the channels 2, 3 and 4 to reflectance. The low mid-infrared reflectance of both snow and water resulted in a loss of the information in the channels 5 and 7 after calibration (too close to noise level).

constant within the test site, but terrain elevation may have influenced the irradiance through varying atmospheric path length. Although a correction for path radiance is implicit in the calibration method, the term *apparent reflectance* is used in the following.

Meteorological observations (wind speed, air temperature, precipitation, and solar radiation recorded every 30 minutes) and manual snow measurements (depth and density) (Figure 3), provided by the Swiss Federal Research Institute WSL, served to estimate the snow conditions at the time of the satellite passes. Repetitive freeze-thaw metamorphoses caused coarse-grained snow on both 10 February and 13 March 2000. For the 10 February 2000 TM acquisition, there was probably an isothermal multi-layered snow pack at 0°C with a thin, frozen surface crust, caused by daily air temperatures above 0°C and freezing night air temperatures. During the three preceding days 30.6 mm precipitation fell presumably as rain, as air temperatures were up to 8°C. Strong winds also favored snow-free tree crowns. On 13 March 2000 the snow pack was also estimated to be at 0°C, thus containing liquid water. During the three days preceding the 13 March TM acquisition the air temperatures fluctuated between −0.9°C and 12°C. The last precipitation event (10 mm) occurred on 10 March, presumably as rain, as air temperatures were 3° to 5°C. At the time of the satellite pass the air temperature was 5.6°C. The tree crowns were therefore assumed to be snow free.

A digital forest fraction map with pixels corresponding to Landsat TM pixels in size (30 m × 30 m) and location was generated from a true color, aerial orthophoto with 0.8 m × 0.8 m pixel size (1:30000 original scale). The aerial photo was acquired on 12 March 1998 for snow-free conditions. Threshold techniques were applied on the green channel of the aerial photo to create a binary image of tree crown pixels and pixels of other surfaces. The tree crown area fraction (A_S) for each corresponding Landsat TM pixel was calculated by aggregating the pixels of the aerial photo, which had been classified as tree crowns.

Precise geocoding is crucial for all subpixel analysis combining different data sets. The accuracy of the rectified Landsat TM images was evaluated qualitatively and quantitatively. Qualitative tests included vector overlaying of lakes, rivers, and forest from thematic maps on the rectified images. Quantitative tests included map coordinate comparison between the images, and validation by a study of residual errors in the ground control points (GCPs) and check points applied in the orthoimage generation. The GCPs were evenly distributed in the Landsat images, and additional points were used as check points to evaluate the geocoding in the study area. A *leave-one-out* method was employed to evaluate the Root Mean Square Error (RMSE) of each GCP, by transforming single GCPs to check points and then calculate RMSE for this check point. Combined x and y errors were approximately 24 m for the GCPs and 30 m for the check points for both Landsat TM images (Table 2). This represents an average displacement of 0.8–1 pixel. The accuracy of the geocoded aerial photo was within few meters.

TABLE 2. ACCURACY OBTAINED FOR THE GROUND CONTROL POINTS (GCPS) AND THE CHECK POINTS (CPS) DURING THE ORTHOIMAGE GENERATION OF THE LANDSAT TM IMAGES. THE ACCURACY (METERS) IS GIVEN FOR $\sqrt{(x^2 + y^2)}$ AND, x AND y SEPARATELY. ACCURACY ESTIMATES FOR THE CHECK POINTS WERE OBTAINED BY THE "LEAVE-ONE-OUT"-METHOD

Date	GCP (x, y)	GCP (x)	GCP (y)	CP (x, y)	CP (x)	CP (y)
10 February 2000	25.2	20.6	14.6	31.2	24.8	18.9
13 March 2000	24.0	14.5	19.2	29.5	18.2	23.3

Experiments and Results

Three experiments were carried out with the data set and are presented successively in this section. The first experiment is calibration of the *TopoSnow* and the *TopoTree* models based on an analysis of radiometric terrain effects from snow and spruce forests. The second experiment is reflectance modeling with the *SnowFor* model with and without these calibrated topographic reflectance models. The third experiment is an evaluation of the four topographic correction methods applied on a test image of snow and spruce forests. The two visible channels, TM2 and TM3, were highly correlated. Therefore, figures and tables include only TM3.

Calibration of the TopoSnow and the TopoTree Models

For the purpose of calibrating the *TopoSnow* and *TopoTree* models, radiometric terrain effects from snow and spruce forests were examined for the visible and the near-infrared channels (TM2–4) of the two Landsat TM scenes (10 February and 13 March 2000). Pure pixels of unforested snow-covered areas (1,843 Landsat TM pixels) and densely forested areas (1,163 Landsat TM pixels) located at varying terrain expositions outside, but close to the 2.76 km × 1.44 km test site were selected. These areas were located approximately 0.3–6.0 km from the test site. The reason for choosing areas outside the test site for the model calibration was to use independent data sets for validation of the *SnowFor* model (see the experiment on reflectance modeling). Maximum terrain slope and the respective terrain azimuth angle were derived for each pixel from the DEM. Using these terrain parameters and the solar elevation and azimuth angles at the image acquisition time, cos(i) was calculated for each pixel according to Equation 1. The solar elevation angles were 23.3° on 10 February and 34.9° on 13 March 2000, the respective solar azimuth angles were 150.2° and 146.8°.

Radiometric terrain effects for snow and dense spruce forests are clearly illustrated in Figure 6. The effects are larger for snow than for spruce forest, and are particularly pronounced for slopes located parallel to the solar illumination plane. Analogous terrain effects were obtained for dense spruce forests and snow in both Landsat TM scenes, but with slightly stronger effects on 10 February 2000. In general, the magnitude of the terrain effects are related to the magnitude of the true reflectance of snow and spruce forests in TM3 and TM4 (Figure 5). Thus, the terrain effects become larger as the true reflectance of a target becomes higher.

The *TopoSnow* and the *TopoTree* models were calibrated from scatterplots of cos(i) and observed visible and near-infrared apparent reflectance for snow and dense spruce

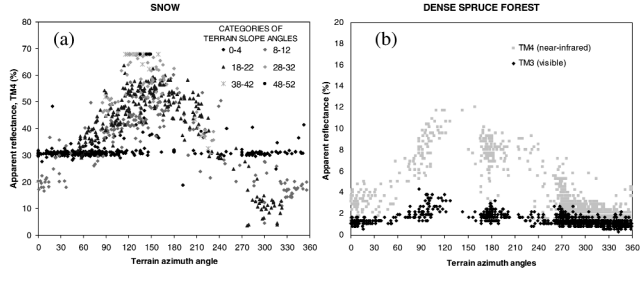

Figure 6. Influence of topography on the apparent reflectance of: a) snow; and b) dense forest, 10 February 2000. Increasing terrain slope angles amplify the variability of apparent reflectance of snow for terrain azimuth angles in the directions close to the solar-illumination plane (solar azimuth angle = 150.3°).

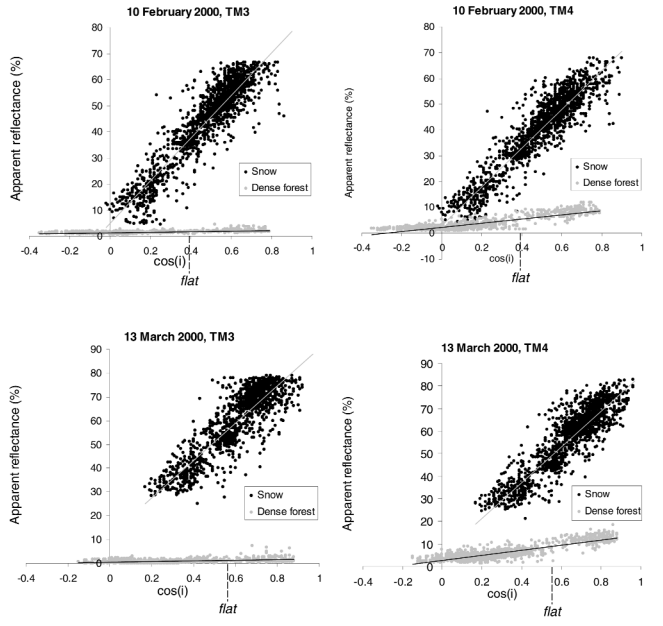

Figure 7. Scatterplots of the local solar incidence angle and apparent reflectance for snow and dense forest, respectively. The *TopoSnow* and *TopoTree* models were calibrated from this data set (see regression equations in Table 3). The solar incidence angles for flat (horizontal) terrain are displayed.

forests (Figure 7). Areas located in shadows have cos(i) values less than zero. Distinct characteristics related to linearity and separability are seen in the scatterplots. The apparent reflectance of snow, and also dense spruce forests, display strong linear dependence on the cos(i). Therefore, the *TopoSnow* (R_{SW}) and the *TopoTree* (R_S) models were calibrated through linear regressions (Table 3), where cos(i) explained up to 86 percent and 76 percent of the variance in the apparent reflectance for snow and dense spruce forests, respectively. Thus, for this data set the direct radiation and land-cover specific reflectance are the main causes of variability in the apparent reflectance as illustrated in Figure 2. Since a linear model was applied, and no other non-linear models better fitted the data set, a Lambertian model was considered an appropriate approximation both for spruce forests and for snow for the studied situations. Snow has been observed to reflect anisotropically, especially in the forward direction (specular reflectance) (Steffen, 1987; Winther, 1993). Forests have been observed with a scattering peak in the backward direction (e.g., Deering, *et al.*, 1999). The illumination-terrain-sensor geometry did not include extreme specular angles in the solar-illumination plane, since all pixels were nearly observed in nadir. The remaining scatter may be explained by secondary effects such as spatial variability of the snow surface (liquid water content, grain size, impurities), cast shadows from adjacent terrain and some anisotropic reflectance of snow and tree crowns.

The ability to map snow depends on the spectral separability between the snow and other surfaces. As seen in Figure 7 the spectral separability between the two clusters of dense spruce forests and snow enlarges with increasing cos(i) values for visible and near-infrared wavelengths. The Jeffries-Matusita measure (Richards, 1993, p. 250) was applied to quantify the spectral separability between these two clusters for defined categories of cos(i), divided into 0.1 intervals (cos(i) = 0–0.09, 0.10–0.19, etc.). For both Landsat TM scenes, the two clusters were highly separable in visible and near-infrared. Even for the lowest cos(i) values the Jeffries-Matusita separability measure showed 2.0, indicating high separability between classes. This separability test supports the division into separate topographic reflectance models for snow and forests.

Reflectance Modeling

Reflectance modeling with the *SnowFor* model was carried out for forests with full snow cover located within the 2.76 km × 1.44 km test site (4,416 Landsat TM pixels). Landsat TM reflectance values were modeled for the visible and the near-infrared channels (TM2–4) for 10 February and 13 March 2000 (Equation 2, Figure 1). Overall, spruce was the dominant species, and minor occurrences of other tree-species were either mapped as spruce or not successfully mapped by the aerial photo. Therefore, completely snow-covered spruce forest was modeled by ignoring the pine component, the birch component, and the bare ground component: $A_P = A_B = A_{BG} = 0$, $A_{SW} + A_S = 1$. The relative area of spruce tree crowns (A_S) for each pixel was taken from the forest fraction map. To study the importance of including radiometric terrain effects in the *SnowFor* model, two tests of reflectance modeling were performed. In the first test, terrain effects were ignored by modeling constant snow reflectance (R_{SW}) and spruce tree-crown reflectance (R_S) for all pixels of an image channel. Average reflectance values were determined from pixels of pure snow or dense spruce forests located in horizontal terrain closely outside the test site (Table 4). For the TM images of 10 February and 13 March 2000, horizontal terrain corresponded to cos(i) = 0.39 and cos(i) = 0.57, respectively. In the second test, terrain effects were included by integrating the calibrated *TopoSnow* and T*opoTree* models as the snow reflectance (R_{SW}) and the spruce tree-crown reflectance (R_S) in the *SnowFor* model (Table 3).

Modeled Landsat TM reflectance ($\hat{R}$) was evaluated against the observed Landsat TM reflectance (R) for the visible and the near-infrared channels. Linear regression models gave estimates of how well the modeled reflectance fits the observed reflectance. Without accounting for topography the modeling results were rather poor, with R^2 values ranging from 0.30 to 0.37. When terrain effects were included the R^2 values

TABLE 3. *TOPOSNOW* AND *TOPOTREE*: CALIBRATED TOPOGRAPHIC REFLECTANCE MODELS FOR SNOW ($R_{SW,\lambda}$) AND SPRUCE TREE CROWNS ($R_{S,\lambda}$). λ IS LANDSAT TM3 AND TM4

	10 February 2000		13 March 2000	
Surface	Equation	R^2	Equation	R^2
Snow	$R_{SW,TM3} = 81.89 \cos(i) + 5.04$	0.85	$R_{SW,TM3} = 79.73 \cos(i) + 11.11$	0.76
	$R_{SW,TM4} = 75.17 \cos(i) + 3.00$	0.86	$R_{SW,TM4} = 79.43 \cos(i) + 5.08$	0.80
Spruce	$R_{S,TM3} = 1.10 \cos(i) + 1.23$	0.38	$R_{S,TM3} = 1.18 \cos(i) + 0.61$	0.16
	$R_{S,TM4} = 8.10 \cos(i) + 2.25$	0.76	$R_{S,TM4} = 11.34 \cos(i) + 2.69$	0.75

TABLE 4. AVERAGE REFLECTANCE VALUES FOR SNOW ($R_{SW\lambda}$) AND SPRUCE TREE CROWNS ($R_{S\lambda}$) FOR HORIZONTAL TERRAIN. λ IS LANDSAT TM3 AND TM4

Surface	10 February 2000	13 March 2000
Snow	$R_{SW,TM3} = 35.8$ $R_{SW,TM4} = 30.8$	$R_{SW,TM3} = 53.6$ $R_{SW,TM4} = 45.4$
Spruce	$R_{S,TM3} = 1.7$ $R_{S,TM4} = 5.4$	$R_{S,TM3} = 1.3$ $R_{S,TM4} = 9.4$

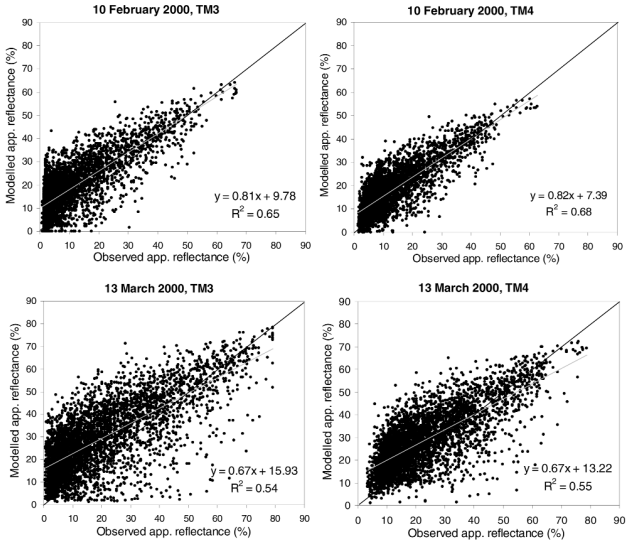

Figure 8. Modelled ($\hat{R}$) and observed (R) Landsat TM3 and TM4 apparent reflectance from 10 February and 13 March 2000. The reflectance modeling includes the calibrated *TopoSnow* and *TopoTree* models. Results are evaluated by linear regression.

improved, ranging from 0.54 to 0.68 (Figure 8). For both dates and TM channels the modeled reflectance is for the most part overestimated for pixels with low reflectance values and underestimated for pixels with high reflectance values, when comparing to an ideal 1:1 model. The R^2 values were higher on 10 February than on 13 March, for visible and near-infrared reflectance. The best model fit was obtained for the near-infrared channel on 10 February ($R^2 = 0.68$). A possible reason for higher model fit on 10 February may be related to stronger model fit of the *TopoSnow* and *TopoTree* models on this date. Error sources in the reflectance modeling are discussed in a later section.

Evaluation of Topographic Correction Methods for Snow and Forests

There is no topographic correction method generally accepted by the scientific community for all applications. Four commonly used methods (Lambertian cosine correction, C-correction, Statistic-empirical correction, and Minnaert correction) were evaluated in this experiment. These methods aim to normalize the illumination of each pixel to flat terrain by making the pixel reflectance independent of the local solar incidence angle *i*.

An experiment was set up to analyze the performance of these methods for snow-covered spruce forests. For this purpose the TM3 and TM4 channels of the 10 February 2000 TM scene were applied. To analyze pure land cover types, the same regions of snow-covered open areas and dense forests as those used to calibrate the *TopoSnow* and the *TopoTree* models were selected to form a test image. Topographic corrections of this test image were carried out with the four methods (Table 1). Empirical parameters required for the C-correction and Statistic-empirical correction were first derived by linear regression of cos(*i*) and apparent reflectance using all the snow and the dense forest pixels in the test image (Table 5). Deriving these parameters using all pixels simultaneously represents common user practice for these methods. Therefore, the parameters are here referred to as ensemble parameters. Next, the procedure was compared with a procedure deriving empirical parameters from specific spectral land cover types, here referred to as land cover specific parameters. Hence, parameters for snow were determined from open snow-covered areas, and parameters for spruce were determined from areas covered by dense forests. This second approach corresponds to the approach applied in calibrating the *TopoSnow* and *TopoTree* models. Following the methodology in Smith, *et al.* (1980), Minnaert constant was determined for: 1) Snow; 2) Dense spruce forest; and 3) Mixture of snow and dense spruce forest. The two former are land cover specific parameters. The latter is ensemble parameter.

TABLE 5. EMPIRICAL PARAMETERS FOR THE TM4 CHANNEL FROM 10 FEBRUARY 2000 APPLIED IN C-CORRECTION, STATISTIC-EMPIRICAL CORRECTION AND MINNAERT CORRECTION OF A TEST IMAGE OF SNOW AND DENSE FOREST. E IS ENSEMBLE PARAMETERS AND C IS LAND-COVER SPECIFIC PARAMETERS. THE LAND-COVER SPECIFIC PARAMETERS *b* AND *m* FOR SNOW AND DENSE FOREST ARE DERIVED FROM THE *TOPOSNOW* AND THE *TOPOTREE* MODELS (TABLE 3). *k* IS THE MINNAERT CONSTANT

Empirical Parameters		*b*	*m*	$C = b/m$	$\bar{L}_T$	*k*
Snow and dense forest	E	4.30	59.66	0.07	24.81	1.06
Snow	C	3.00	75.17	0.04	38.32	0.84
Dense forest	C	2.25	8.10	0.28	3.41	0.45

Results of the topographic corrections of the test image, using ensemble parameters and land cover specific parameters, are shown in Figures 9 and 10. Results are presented separately for the snow and the forest areas. Similar results were obtained for both TM3 and TM4 channels of the 10 February image. Therefore, only the TM4 channel is displayed in Figures 9, 10 and Table 5. Generally, the Lambertian cosine correction over-corrects significantly for low cos(*i*) values due to near-zero division (Figure 9). This observation is earlier described by Teillet, *et al.* (1982), Meyer, *et al.* (1993) and Ekstrand (1996). Areas with cos(*i*) values less than zero are

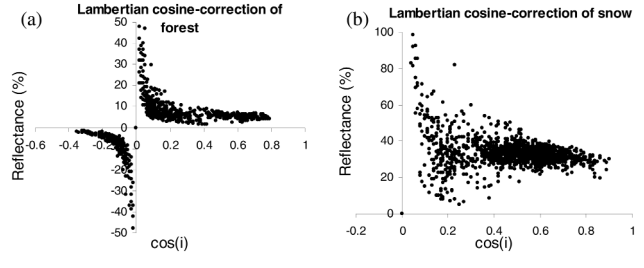

Figure 9. Lambertian topographic correction method applied on a test image composed of pure snow and dense forest pixels. Topographic corrected areas of dense forest (a) and snow (b) are illustrated separately. Only the TM4 channel from 10 February 2000 is shown. Negative apparent reflectance values are included for illustration, but will in practice be set to 0.

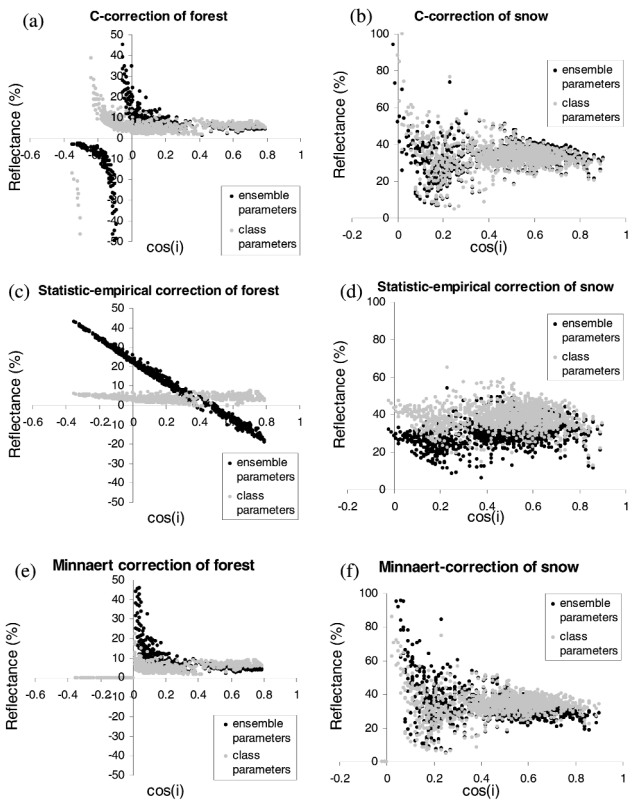

Figure 10. Comparison of topographic correction methods applied on the same data set as presented in Figure 9. The results of using both the ensemble parameters and the land-cover specific (class) parameters from Table 5 are shown. Using land-cover specific parameters means that snow areas and forest areas were corrected by applying empirical parameters derived for snow and forests, respectively. Negative apparent reflectance values are included for illustration, but will in practice be set to 0.

located in shadows. To avoid the over-correction these areas are commonly set to zero reflectance or excluded from the analysis. The C-correction is a modification of the Lambertian cosine correction, which displaces the over-correction towards lower cos(*i*) values. The effect is very well illustrated for forest in Figure 10a. The results for the forest areas are further improved when land cover specific parameters are applied in C-correction as compared to ensemble parameters. The Statistic-empirical correction gives quite large errors for the forest areas when using ensemble parameters, while land cover specific parameters provide the overall best correction results for forests (Figure 10c). Generally, the snow pixels are much more scattered than the forest pixels, and best correction results are also obtained with the Statistic-empirical correction using land cover specific parameters. Although the Minnaert constant was estimated for specific land cover types, the results of this correction were generally weak, with some improvements over the Lambertian cosine correction for forest. As shown in Table 5 the Minnaert constant is strongly surface dependent. The ensemble parameter for Minnaert constant ($k = 1.06$) becomes too large because it is determined from a data set including two land cover types (snow and spruce forest) with quite different reflectance. Values of the Minnaert constant have previously been suggested for pine (Smith, *et al.*, 1980; Colby, 1991), spruce (Ekstrand, 1996) and snow (Ronald Eyton, 1989).

In summary, best results were obtained using land-cover specific parameters. For forests, the methods were ranked in the following order, based on the results: 1) Statistic-empirical correction; 2) C-correction; 3) Minnaert correction; and 4) Lambertian cosine correction. For snow, best results were also obtained with the Statistic-empirical correction, using land-cover specific parameters. The other methods were difficult to rank for snow.

Discussion

The results show that the use of *TopoSnow* and *TopoTree* enhance the modeling of reflectance variability from snow-covered forests. To explain the errors in the reflectance modeling that still remained after having included terrain effects, a thematic analysis of the errors was carried out. From modeled and observed reflectance values for every pixel, absolute errors ($\varepsilon_{abs} = \hat{R} - R$) and relative errors ($\varepsilon_{rel} = (\hat{R} - R)/R$) were computed. The aim was to search for sources of large errors, and to look for systematic errors. The topics of the discussion are the proportions of snow and trees within a pixel, the solar incidence angle, the terrain relief effects, and, the importance of land cover specific models.

Proportions of Snow and Trees within a Pixel

A possible relationship between the reflectance modeling error and the proportions of snow and trees within a pixel was investigated. Pixels used in the reflectance modeling (4,416 pixels) were divided into categories based on their tree-crown area percentage, which means that every category includes pixels having a wide range of local solar incidence angles. Average and standard deviation of both absolute and relative errors were estimated for each category (Figure 11). Positive average values represent overestimation of the reflectance, while negative values represent underestimation. The plots of absolute errors indicate a relationship to the true reflectance of a land cover type. The largest errors occur in sparsely forested areas where the major contribution to pixel reflectance stems from snow, while the lowest errors are obtained for relatively dense forests (80–89 percent tree crown area).

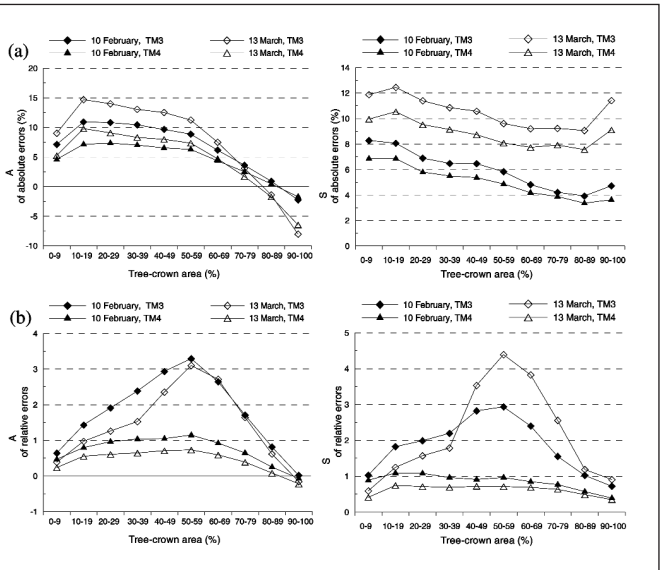

Figure 11. Average and standard deviation of: a) the absolute errors ($\varepsilon_{abs} = \hat{R} - R$, %); and b) the relative errors ($\varepsilon_{rel} = (\hat{R} - R)/R$). Pixels are divided into categories of tree-crown area percentage, where 0% means unforested area with full snow-coverage.

Relative errors were computed to avoid the relationship between absolute errors and true reflectance of snow and spruce forests, and thereby perhaps reveal other error sources. As observed in Figure 11b the relative errors are small for areas of pure snow or spruce forests. Both the average and the standard deviation of relative errors increase when the two land cover types mix, with a maximum error when the mixture consists of 50 percent of each type. This effect is significantly larger for the visible (TM3) than for the near-infrared (TM4) channel on both 10 February and 13 March 2000. However, the data set used in this study is not sufficiently large to judge whether these observations are arbitrary or systematic.

Local Solar Incidence Angle

To study errors arising from changing local solar incidence angle, i, within the test site, all pixels were divided into categories based on their cos(i) value. In this manner every cos(i) category includes unforested, sparsely and densely forested pixels. Average and standard deviation of the relative errors (ε_{rel}) for each category is shown in Figure 12. A wavelength dependent trend is observed in the plots. The relative errors for the near-infrared channel (TM4) are rather independent of the solar incidence angle, while for the visible channel (TM3) the relative errors increase with cosine of the solar incidence angle. Hence, the more direct radiation a pixel receives the higher the errors become, which may indicate that some terrain effects still remain for the visible channel.

In summary, the thematic analysis of absolute and relative errors suggests that more sophisticated modeling of particularly shadow effects (reflected diffuse illumination, cast shadows from trees, and adjacent terrain) is necessary to improve the reflectance modeling results. Inclusion of individual shadow effects has been attempted with single-tree modeling for flat terrain by Vikhamar and Solberg (2003b). The cause for the overall larger relative errors for the visible channel (TM3) as compared to the near-infrared channel (TM4) may be that shadow effects are more important for visible than for near-infrared wavelengths.

Terrain Relief Effects

The terrain relief may influence the results in several ways: 1) The calculation of terrain parameters (slope and azimuth), and thereby the computed local solar incidence angle, depend on the accuracy of the DEM. The accuracy of the DEM used in this analysis was 3–5 m (Swisstopo, 1999), and considered good for the purpose. Still, a DEM with higher spatial resolution than 25 m would improve the terrain parameter calculation due to better representation of the terrain relief. 2) The geometric co-registration of the DEM, the satellite images and the aerial photo is crucial for the results, and depends on the terrain relief roughness. A geometric displacement of one pixel would have larger influence for areas with steep relief than for areas with smooth relief. The geometric accuracy of the Landsat TM images was 0.8-1 pixel (see description of the data set). 3) The local solar incidence angle was calculated from a DEM representing the terrain relief. If there was a difference between the terrain relief and the *canopy relief*, the local solar incidence angle may have been inaccurately computed for areas with dense forest, but this effect is considered small.

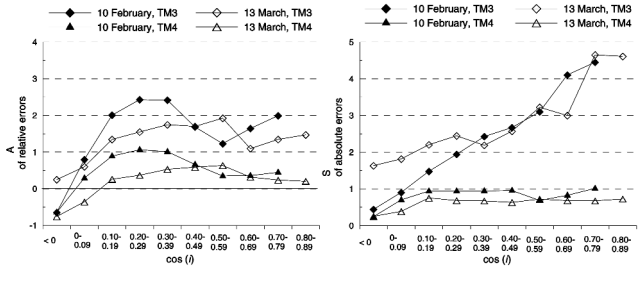

Figure 12. Average and standard deviation of the relative errors ($\varepsilon_{rel} = (\hat{R} - R)/R$). Pixels are divided into categories of local solar incidence angle, based on the cos(i) values. Each category, therefore, encompasses various ranges of tree-crown area percentage.

Land Cover Specific Models

The evaluation of four topographic correction methods revealed that the three methods requiring empirical parameters give best results when land-cover specific parameters are applied. The focus on forests with relatively homogeneous reflectance properties is a reason why e.g., Meyer, *et al.* (1993) obtained good results using the C-correction and the Statistic-empirical correction. The experiment in this work demonstrates the sensitivity of these methods to land-cover types. Since land cover types with both low (forest) and high (snow) true reflectance where examined, the extreme effects are illustrated. In summary, these methods may give appropriate results for visible and near-infrared images of either snow or forests, if land cover specific parameters are applied. The performance of these methods is low for mixed pixels of snow and forests. The reason is the large spectral difference between snow and spruce forests in these wavelengths.

The four topographic correction methods are not directly comparable with the *TopoTree* and the *TopoSnow* models because the former removes the terrain effects, while the latter includes terrain effects. Therefore, no quantitative comparison was carried out. The motivation for proposing an approach, which includes rather than removes the terrain effects, is based on the purpose of the reflectance modeling, which is improved snow-cover mapping in forests by spectral unmixing using the *SnowFor* linear spectral mixture model. For the *SnowFor* model, terrain effects should be accounted for by every land cover reflectance component and not for the entire observed pixel reflectance. It was clearly demonstrated in Figures 6 and 7 that terrain effects depend on land cover type and influence differently for snow and spruce forests. It was also shown in Figures 9 and 10 that the evaluated topographic correction methods are improved when they are adapted to specific land cover types, but still these methods correct the entire observed pixel reflectance and not subpixel land cover reflectance components.

Conclusions and Outlook

To map the snow in forests, the primary factors, trees, snow-free bare ground, wavelength and topography should be accounted for. For this purpose Vikhamar and Solberg (2002 and 2003b) previously developed the *SnowFor* linear spectral mixture model described for snow, trees and bare ground in flat terrain. In this paper, the *SnowFor* model is extended by accounting for topography. Terrain effects are not removed from the observed pixel reflectance but included for every reflectance component of the *SnowFor* model. Two submodels (*TopoSnow* and *TopoTree*) are proposed for modeling the reflectance from snow and tree-crowns, respectively.

Experiments with two Landsat TM images of hilly, forested terrain with full snow coverage (Alptal, Switzerland) show that the calibrated *TopoSnow* and *TopoTree* models improve the modeling of reflectance variability from snow-covered forests. Modeled and observed Landsat TM visible and near-infrared reflectance were compared with and without the *TopoSnow* and the *TopoTree* models. When terrain effects were included in the *SnowFor* model, the R^2 values were considerably improved from 0.30–0.37 to 0.54–0.68.

Finally, the performance of four extensively used topographic correction methods was examined for snow-covered forests (Lambertian cosine correction, C-correction, Statistic-empirical correction, and Minnaert correction). The importance of using land cover specific parameters was demonstrated for snow and dense forests for the visible and near-infrared channels. The performance of these methods is low for mixed pixels of snow and forests due to large differences in true reflectance of snow and spruce forests in these wavelengths. Therefore, terrain effects should be handled for every reflectance component in the *SnowFor* linear spectral mixture model, as was attempted in this study with the *TopoSnow* and *TopoTree* models.

Experiences from this work will allow improved snow-cover mapping with the *SnowFrac* method (Vikhamar and Solberg, 2003a). MODIS images are currently most suitable for operational snow-cover mapping based on *SnowFrac*. Spectra of snow and forests are required to map snow in forests by spectral unmixing. For this purpose calibrated functions for *TopoSnow* and *TopoTree* may be generated for image channels which are sensitive to terrain effects, as shown in this study, for visible and near-infrared wavelengths. The results from the two TM scenes demonstrate that the terrain modifies the spruce forest reflectance less than the snow reflectance. For winter conditions the natural reflectance variability of spruce trees is also less than for snow. This opens the possibility to derive a single generalized *TopoTree* function for every terrain-sensitive channel for use on other scenes to map snow with *SnowFrac*. For the same reasons, generalized *TopoSnow* functions for a few defined snow types (dry, wet, fresh, and old snow) for terrain-sensitive channels may be derived. The snow type of a scene may be inferred from meteorological data. As an alternative to the empirical approach presented in this study, physical models handling both topography and spectral classes (BRDF models of snow and forests) also represent an interesting approach for future research on snow-cover mapping of forested areas, as well as for other applications.

Acknowledgments

This research was financed by the Department of Geosciences, University of Oslo, Norway and the Remote Sensing Group, Computer Vision Lab, ETH, Switzerland. The Landsat data was provided by the NPOC (Swiss national archive center for satellite images). The Swiss Federal Office of Topography provided the digital elevation model and the aerial photo. Snow measurements and meteorological observations have been made available by the Swiss Federal Research Institute WSL. Thanks to Manfred Stähli for geocorrecting the aerial photo, and to Bengt Lundén, Thomas Schuler, and Jesko Schaper for help and fruitful discussions.

References

Andersen, T., 1982. Operational snow mapping by satellites, International Association of Hydrological Sciences *IAHS Publication*, Volume 138, pages 149–154.

ASD, 1996. *FieldSpec Users Guide*, Technical report, Analytical Spectral Devices, Boulder, Colorado, U.S.A.

Cess, R.D., G.L. Potter, M.H. Zhang, J.P. Blanchet, S. Chalita, R. Colman, D.A. Dazlich, A.D. Del Genio, V. Dymnikov, V. Galin, D. Jerrett, E. Keup, A.A. Lacis, H. Le Treut, X.Z. Liang, J.F. Mahfouf, B.J. McAvaney, V.P. Meleshko, J.F.B. Mitchell, J.J. Morcrette, P.M. Norris, D.A. Randall, L. Rikus, E. Roeckner, J.F. Royer, U. Schlese, D.A. Sheinin, J.M. Slingo, A.P. Sokolov, K.E. Taylor, W.M. Washington, R.T. Wetherald, and I. Yagai, 1991. Interpretation of snow-climate feedback as produced by 17 general circulation models, *Science*, 253:888–892.

Colby, J.D., 1991.Topographic normalization in rugged terrain, *Photogrammetric Engineering & Remote Sensing*, 57(5):531–537.

Deering, D.W., T.F. Eck, and B. Banerjee, 1999. Characterization of the reflectance anisotropy of three boreal forest canopies in spring-summer, *Remote Sensing of Environment*, 67(2):205–229.

Dymond, J.R., J.D. Shepherd, and J. Qi, 2001. A simple physical model of vegetation reflectance for standardising optical satellite imagery, *Remote Sensing of Environment*, 77(2):229–239.

Ekstrand, S., 1996. Landsat TM-based forest damage assessment correction for topographic effects, *Photogrammetric Engineering & Remote Sensing*, 62(2):151–161.

Foster, J.L., A.T.C. Chang, and D.K. Hall, 1997. Comparison of snow mass estimates from a prototype passive microwave snow algorithm, a revised algorithm and a snow depth climatology, *Remote Sensing of Environment*, 62:132–142.

Gemmel, F., 1998. An investigation of terrain effects on the inversion of a forest reflectance model, *Remote Sensing of Environment*, 65:155–169.

Gu, D., and A. Gillespie, 1998. Topographic normalization of Landsat TM images of forest based on subpixel sun-canopy-sensor geometry, *Remote Sensing of Environment*, 64(2):166–175.

Hall, D.K., J.L. Foster, V.V. Salomonson, A.G. Klein, and J.Y.L. Chien, 2001. Development of a technique to assess snow-cover mapping errors from space, *IEEE Transactions on Geoscience and Remote Sensing*, 39(2):432–438.

Hall, D.K., G.A. Riggs, and V.V. Salomonson, 1995. Development of methods for mapping global snow cover using Moderate Resolution Imaging Spectroradiometer data, *Remote Sensing of Environment*, 54(2):127–140.

Hall, D.K., G.A. Riggs, V.V. Salomonson, N.E. DiGirolamo, and K.J. Bayr, 2002. MODIS snow-cover products, *Remote Sensing of Environment*, 83:181–194.

Hallikainen, M., 1989. Microwave radiometry of snow, *Advances in Space Research,* 9(1):(1)267–(1)275.

Klein, A.G., D.K. Hall, and G.A. Riggs, 1998. Improving snow cover mapping in forests through the use of a canopy reflectance model, *Hydrological Processes*, 12(10–11):1723–1744.

Koskinen, J.T., J.T. Pulliainen, and M.T. Hallikainen, 1997. The use of ERS-1 SAR data in snow melt monitoring, *IEEE Transactions on Geoscience and Remote Sensing*, 35(3):601–610.

Li, X., and A.H. Strahler, 1985. Geometric-optical modeling of a conifer forest canopy, *IEEE Transactions on Geoscience and Remote Sensing*, GE-23(5):705–721.

Metsämäki, S., J. Vepsäläinen, J. Pulliainen, and Y. Sucksdorff, 2002. Improved linear interpolation method for the estimation of snow-covered area from optical data, *Remote Sensing of Environment*, 82:64–78.

Meyer, P., K.I. Itten, T. Kellenberger, S. Sandmeier, and R. Sandmeier, 1993. Radiometric corrections of topographically induced effects on Landsat TM data in an Alpine environment, *ISPRS Journal of Photogrammetry and Remote Sensing*, 48(4):17–28.

Minnaert, M., 1941. The reciprocity principle in lunar photometry, *Astrophysical Journal*, 93:403–410.

Nagler, T., and H. Rott, 2000. Retrieval of wet snow by means of multitemporal SAR data, *IEEE Transactions on Geoscience and Remote Sensing*, 38(2):754–765.

Pouch, G.W., and D.J. Campagna, 1990. Hyperspectral direction cosine transformation for separation of spectral and illumination information in digital scanner data, *Photogrammetric Engineering & Remote Sensing*, 56(4):475–479.

Proy, C., D. Tanré, and P.Y. Deschamps, 1989. Evaluation of topographic effects in remotely sensed data, *Remote Sensing of Environment*, 30:21–32.

Richards, J.A., 1993. *Remote sensing digital image analysis: An introduction*, Springer-Verlag, Berlin, Germany.

Ronald Eyton, J., 1989. Low-relief topographic enhancement in a Landsat snow-cover scene, *Remote Sensing of Environment*, 27:105–118.

Rosenthal, W., and J. Dozier, 1996. Automated mapping of montane snow cover at subpixel resolution from the Landsat Thematic Mapper, *Water Resources Research*, 32(1):115–130.

Salisbury, J.W., 2002. Johns Hopkins University Spectral Library and ASTER Spectral Library, URL: http://speclib.jpl.nasa.gov/ (last date accessed: 28 June 2004).

Schott, J.R., 1997. *Remote sensing: The image chain approach*, Oxford University Press, New York, USA.

Smith, J.A., T.L. Lin, and K.J. Ranson, 1980. The Lambertian assumption and Landsat data, *Photogrammetric Engineering & Remote Sensing*, 46(9):1183–1189.

Solberg, R., and T. Andersen, 1994. An automatic system for operational snow-cover monitoring in the Norwegian mountain regions, In *Proceedings of IGARSS 1994 Symposium*, pages 2084–2086, Pasadena, California, USA. IEEE.

Solberg, R., D. Hiltbrunner, J. Koskinen, T. Guneriussen, K. Rautiainen, and M. Hallikainen, 1997. Snow algorithms and products—Review and recommendations for research and development, *NR Report No. 924*, Norwegian Computing Center, Oslo, Norway.

Song, C., C.E. Woodcock, K.C. Seto, M.P. Lenny, and S.A. Macomber, 2001. Classification and change detection using Landsat TM data: When and how to correct atmospheric effects?, *Remote Sensing of Environment*, 75:230–244.

Steffen, K., 1987. Bidirectional reflectance of snow at 500–600 nm, *International Association of Hydrological Sciences–IAHS Publication*, Volume 166, pages 415–425.

Swisstopo, 1999. Digital Height Model–DHM25, *Product information*, Swiss Federal Office of Topography, Bern, Switzerland.

Teillet, P.M., B. Guindon, and D.G. Goodenough, 1982. On the slope-aspect correction of multispectral scanner data, *Canadian Journal of Remote Sensing*, 8(2):84–106.

Vikhamar, D., and R. Solberg, 2002. Snow-cover mapping in forests by optical remote sensing: A new reflectance model for snow-covered forests, *NR Report No. 984*, Norwegian Computing Center, Oslo, Norway.

Vikhamar, D., and R. Solberg, 2003a. Snow-cover mapping in forests by constrained linear spectral unmixing of MODIS data, *Remote Sensing of Environment*, 88(3):309–323.

Vikhamar, D., and R. Solberg, 2003b. Subpixel mapping of snow cover in forests by optical remote sensing, *Remote Sensing of Environment* 84(1):69–82.

Winther, J.G., 1993. Landsat TM derived and in-situ summer reflectance of glaciers in Svalbard, *Polar Research*, 12(1):37–55.

Winther, J.G., and D.K. Hall, 1999. Satellite-derived snow coverage related to hydropower production in Norway: Present and future, *International Journal of Remote Sensing*, 20(15–16): 2991–3008.

(Received 12 June 2002; revised and accepted 22 August 2003)